Optics Letters

Domain growth driven by a femtosecond laser in lithium niobate crystal

Xiaoliang Wang,[1] Qiang Cao,[1,*] Ruonan Wang,[1] Xiangdong Cao,[2] and Sheng Liu[1]

[1]The Institute of Technological Sciences, Wuhan University, Wuhan 430072, China
[2]Center for Optics Research and Engineering of Shandong University, Shandong University, Jinan 250100, China
*Corresponding author: caoqiang@whu.edu.cn

Received 4 July 2022; revised 12 December 2022; accepted 15 December 2022; posted 15 December 2022; published 17 January 2023

We experimentally demonstrate to drive domain growth in lithium niobate crystal by using a focused infrared femtosecond laser without relative displacement or any additional treatment. The physical process has four stages: modified domain generation; thermoelectric field formation; domain inversion; and domain growth. The length of domain growth depends on drive energy (pulse energy) and drive time (number of pulses), up to 155 μm. We use this approach to rapidly fabricate two-dimensional period-inverted domain structures and perform frequency-doubling conversion based on quasi-phase-matching. Laser-driven domain growth delivers an efficient manufacturing route for tailored functional materials.

https://doi.org/10.1364/OL.469202

Ferroelectrics are materials that exhibit spontaneous polarization below the Curie temperature and have important applications in nonlinear optics, information storage, photovoltaics, optoelectronic modulation, and quantum communication [1–5]. One of the keys is that the polarization direction and associated domain of such materials can be manipulated [6]. Regions with the same spontaneous polarization direction are referred to as ferroelectric domains, and the boundary between the different spontaneous polarization regions is the domain wall.

The employment of an electric field in excess of the coercive field to invert polarization is now a well-established solution [7], such as the manufacture of the widely used periodically poled lithium niobate (PPLN). However, the electric field poling is cumbersome to operate and has some limitations. For instance, the electric field poling is poor in providing a high aspect ratio of fine-domain periodic PPLN because it causes lateral movement of the domain walls [8]. Since the electric field is applied to both sides of the crystal's surface, domain inversion can only start at the surface and it is not possible to create isolated ferroelectric domains inside the crystal. Moreover, the electric field needs to be along the direction of spontaneous polarization if long domains are to be obtained, which limits the crystallographic orientation of the ferroelectrics. High voltages are required for poling thick samples with high coercive field [9].

Given the benefits of light processing, such as remote manipulation, high resolution, and 3D fabrication capability, the use of light-induced domain inversion as an alternative approach is an active field of research [10]. In related works, the light-assisted electric field poling effectively reduces the coercive field; however, it is the external electric field that remains the main protagonist in causing domain inversion [11]. Through the formation of a thermoelectric or pyroelectric field by high absorption, the UV light poling is able to induce domain inversion without applying an external electric field, but only in the subsurface layer of the crystal [12]. Based on the similar mechanism, the thermoelectric field induced by the thermal gradient generated via nonlinear absorption of a focused near-infrared femtosecond laser in media allows for the direct writing of inverted domain structures inside ferroelectrics [13].

This superior fabrication performance has led to many breakthroughs in nonlinear optics. For example, the fabrication of 3D domain inversion structures in calcium barium titanate, $Ba_{0.77}Ca_{0.23}TiO_3$, calcium barium niobate, and tetragonal PMN-38PT crystals gives access to 3D nonlinear photonic crystals with potential applications in nonlinear beam shaping, nonlinear imaging, and 3D holography [14–17]. Alternatively, domain inversion can also be induced by means of femtosecond laser modification followed by heat treatment [18]. However, using current optical poling methods to fabricate long domain inversion either requires moving the position of the focal spot or needs additional auxiliary processes, which clearly limits the working efficiency of all-optical poling.

In this work, we experimentally demonstrate a new approach for all-optical poling. We show domain inversion growth driven by a focused infrared femtosecond laser in a lithium niobate ($LiNbO_3$) crystal during which no relative displacement and no additional treatment are needed. The length of the domain inversion is dependent on the pulse energy and the number of pulses, up to 155 μm. This technique improves the efficiency of optical poling and is suitable for most ferroelectric materials.

The samples are z-cut 5% MgO-doped $LiNbO_3$ crystal with a thickness of 500 μm. The sample is mounted onto a high-precision displacement holder (Aerotech Inc.) equipped with a PC-driven 3-axis xyz crossed-roller bearing positioning system. A universal femtosecond laser fabrication system is used to drive domain growth. Light is derived from a regenerative amplified Yb:KGW-based laser system (Pharos, Light Conversion) outputting light with a wavelength of 1026 nm, a pulse duration of 170 fs, and a repetition rate of 1000 kHz. The pulse energy can be continuously adjustable from 0 to 400 μJ through an

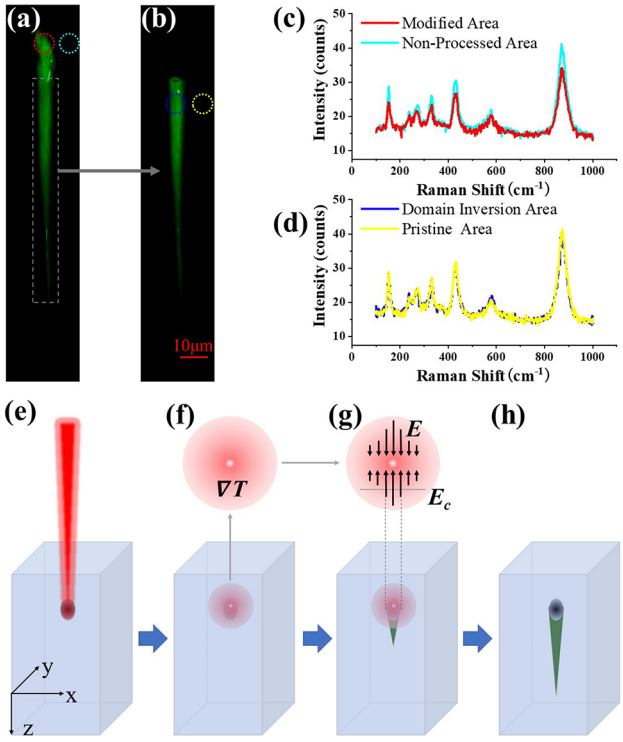

Fig. 1. (a) Domain structure induced by the LDDG (laser-driven domain growth) technique in LiNbO3 crystal and (b) domain inversion region therein, visualized by Čerenkov SH microscopy. The drive energy and time are 500 nJ and 0.5 s, respectively. (c) Micro-Raman signal of the modified domain and non-processed area marked by dashed circles in panel (a). (d) Micro-Raman signal of the domain inversion and pristine area marked by dashed circles in panel (b). The color of the dashed circles corresponds to the color of the Raman signal in their marked regions. (e)–(h) Four physical processes of LDDG: modified domain generation; thermoelectric field formation; domain inversion; and domain growth, respectively.

attenuator consisting of a half-wave plate and a polarizing plate. Focusing the laser with a 50× microscope objective (NA = 0.42) produces a focal spot diameter of approximately 1–2 μm. The light polarization is along the x-direction of the crystal during processing.

After the beam is incident from the −z-surface to a spot inside the crystal, the beam or the sample is not moved and no additional treatments are performed. Driven by the laser, the domain inversion continues from the focal spot toward the inside of the crystal. At the end of the radiation, a modified domain is produced in the focal region and a long-inverted domain is created below the focal spot, and the experimental results are shown in Figs. 1(a) and 1(b). Induced domain structures are observed by Čerenkov-type second harmonics (SH) confocal microscopy (FVMPE-RS, Olympus), allowing for nondestructive characterization [19,20]. Owing to the Čerenkov-type effect, the excited second harmonic is enhanced at the boundary of second-order nonlinearity variations. A sharper change in the second-order nonlinearity results in a more pronounced Čerenkov-type effect. Therefore, inverted and modified domains can be observed. The difference between them is that as the modified domain are irregular, it has SH signal over its entire region. In contrast, only the domain walls have SH signal in the regions of the inverted domains, as shown in Fig. 1(b).

The areas marked in Figs. 1(a) and 1(b) were characterized using micro-Raman and the corresponding results are shown in Figs. 1(c) and 1(d). There is a significant weakening of the Raman signal in the focal areas, which suggests that the laser radiation has changed the chemical structure of this region and may have formed amorphous components [21,22]. The Raman signal in the domain inversion region also shows once again that the laser-driven domain structure only reverses the direction of polarization since the change in polarization direction does not affect the Raman signal.

The physical process of laser-driven domain growth (LDDG) is shown in Figs. 1(e)–1(h). When multiple laser pulses are focused inside the crystal, extremely high temperatures are formed in the focal region due to multiphoton absorption and electron–phonon heat transfer. The high temperature disrupts the crystal structure, thus weakening the nonlinear coefficient in this region producing a modified domain [23], as shown in Fig. 1(e). At high temperatures, the coercive field near the focus may be less than 100 V/mm. The subsequent radiation and thermal diffusion create a high temperature gradient around the modified domain. Owing to the thermoelectric effect, the temperature gradient induces a bipolar thermoelectric field. A higher temperature gradient will result in a stronger thermoelectric field. In case the thermoelectric field is larger than the coercive field, it results in domain inversion, as shown in Figs. 1(f) and 1(g). With a thermoelectric power tensor $Q_{33} = 0.8$ mV/K, the temperature gradient ∇T only needs to be greater than 125 K/μm to invert the spontaneous polarization of the crystal. Thereafter, the domain inversion region conically grows outward under the action of the thermoelectric field and inversion dynamics [24,25], as shown in Fig. 1(h).

In addition, we observed that the pulse energy required for LDDG is necessarily larger than the crystal damage threshold, that is, the laser radiation will inevitably fabricate a modified domain in the focal region. We think this is due to several possibilities, one is that laser poling needs a large area of high temperature to generate enough electric field, while non-destructive multiphoton absorption and heat transfer cannot meet the requirement. Second, the presence of modified domains reduces the coercive electric field because the domain walls trap electrons [26]. Third, the regions around the modified domain may be used as nucleation sites [27–29]. If laser direct writing could induce a domain inversion of arbitrary length in $LiNbO_3$ without damage, then direct writing of 3D-poled $LiNbO_3$ would have been available long ago, instead of being compromised by laser modification [22,30]. Apart from satisfying the pulse energy, a large number of pulses is required for LDDG. For example, in our experiments, a number of pulses greater than 10^4 is desired that accomplish sufficient thermal accumulation to form a stable poling field.

The processes of LDDG are similar to Imbrock's treatments [18], except that we have simplified their laser modification and additional heating to a single step. The inverted domain shape we fabricated is conical, consistent with the results reported by Chen *et al.* [31] using a femtosecond laser to scan inside the crystal. However, we consider that conical domain is an intrinsic property of LDDG, and its mechanism is different from the spherical aberrations and birefringence they attribute to it. In the LDDG, the inverted domain is constantly consuming energy as it grows. The growth of the domain wall requires more energy than the growth of the domain center, resulting in slower growth of the domain wall. This difference in growth rate from the domain

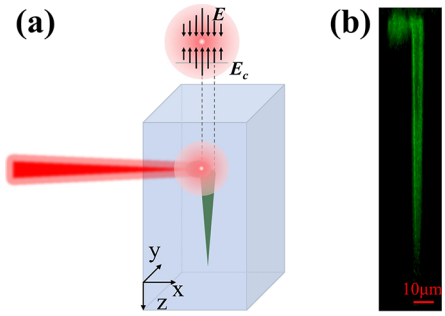

Fig. 2. (a) Schematic and (b) experimental result (Čerenkov SH microscopy image) of the domain growth driven by light incident from the x-surface to the inside of the crystal. The drive energy and time are 500 nJ and 0.5 s, respectively.

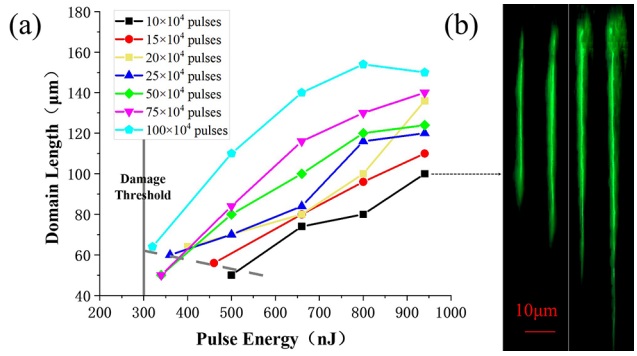

Fig. 3. (a) Length of LDDG for different pulse energies and numbers of pulses. (b) Experimental results (Čerenkov SH microscopy image) of driving domain growth with 10×10^4 pulses and pulse energies of 520, 660, 800, and 940 nJ.

center to the domain wall causes the formation of a conical domain. We drive the domain growth with a laser incident from the x- or y-surface into the crystal, the results are also the same as for the −z-surface incident, as shown in Fig. 2. The region below the focal spot was not irradiated by the light at all, and domain inversion also occurred. Because the nucleation sites tend to appear below the modified domains (at the downstream end of the laser incidence direction), and the inversion domain always grows along the z axis. So, in this case, the modified and inverted domains do not overlap in the z-direction.

We observe that the length of LDDG is governed by drive energy (pulse energy) and drive time (number of pulses). When the laser is focused at 20 μm below the −z-surface, the minimum drive energies to meet the induced domain inversion at different drive times, and the domain length at different drive energies and times, are shown in Fig. 3(a). First, as shown by the gray dashed line, a longer drive time results in a smaller drive energy required to induce domain inversion until it is close to the damage threshold, and accordingly, the domain length increases slightly. There is a minimum value for the length of the LDDG. For example, in our current experiments, the laser either fails to drive a domain inversion or will drive a domain that is at least 50 μm in length, which may be related to the domain inversion dynamics of the crystal. Furthermore, the domain length increases with drive energy and time and is tunable between 50 μm and 155 μm.

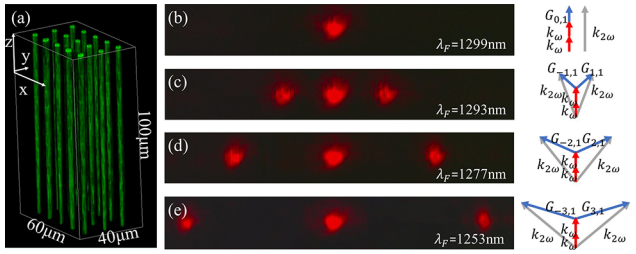

Fig. 4. (a) Čerenkov SH microscopy image of a 2D domain structure fabricated by LDDG technique. The drive energy and time are 700 nJ and 1 s, respectively. (b)–(e) 2D QPM SH patterns at various input fundamental.

Figure 3(b) shows the experimental results of LDDG with a drive time of 0.1 s (10×10^4 pulses) and drive energies of 520, 660, 800, and 940 nJ, respectively. The obtained domain lengths are 50, 74, 80, and 100 μm, respectively. Compared to laser scanning (10 μm/s) [32], the speed of fabricating a 50–100-μm domain with laser drive is 50–100 times faster. Creating other lengths of domains can also improve speed by at least 10 times. We believe that a longer domain and shorter drive time can be realized by co-optimizing other laser parameters, such as wavelength, pulse width, and repetition rate.

The initial diameter of the inverted domain is also positively correlated with the drive energy and time. The main reason is that a high drive energy or a long drive time creates a stronger and wider range of the thermoelectric field, resulting in a larger domain inversion area. In addition, the domain length decreases whenever the depth of focus deepens, as the laser energy is absorbed and the focal spot is distorted. While the laser is incident from the x- or y-surface, the shape of the driven domain growth is almost identical at different z-positions.

Figure 4(a) shows a partial view of a 2D domain structure fabricated with LDDG with a period of $\Lambda x = \Lambda y = 12.5$ μm, a duty cycle of 0.25, and a period number of 80 (x) × 80 (y). The structure ensures approximately the same shape over a length of 100 μm. We performed second harmonic generation (SHG) experiments for demonstrating the 2D quasi-phase matching (QPM) of this structure. The QPM condition is described as

$$k2\omega - 2k\omega - Ga,b = 0, \tag{1}$$

where $k\omega$ and $k2\omega$ are the wave vectors of fundamental and harmonic waves, respectively, Ga,b is the 2D reciprocal lattice vector defined as

$$Ga,b = a\frac{2\pi}{\Lambda x}\hat{x} + b\frac{2\pi}{\Lambda y}\hat{y}, \tag{2}$$

where $\hat{x}$ and $\hat{y}$ are unit vectors, a and b are integers. The experimental SH patterns with input fundamental wavelengths of 1299, 1293, 1277, and 1253 nm are shown in Figs. 4(b)–4(e), respectively. The fundamental beam has a diameter of 50 μm, pulse duration of 270 fs, and repetition rate 300 Hz. The output far-field SH patterns are collected and recorded with a CCD. When the fundamental input power is 5 mW, the conversion efficiency of collinear SHG is approximately 1.4×10^{-3}, and the total conversion efficiency of collinear line and non-collinear SHG is approximately 3.6×10^{-3}. The conversion efficiency can be further improved by increasing the QPM length, raising the fundamental input energy, and optimizing the duty cycle.

To conclude, we have experimentally demonstrated domain growth driven by a focused femtosecond laser in $LiNbO_3$. This approach allows the fabrication of a long inversion domain inside the crystal without additional treatment, without moving the sample or the laser focus. The physical process consists of four stages: domain modification generation; thermoelectric field formation; domain inversion; and domain growth. The modified domain plays an important role, and its possible reduction of the coercive field or as a nucleation site needs to be further studied. The length of the domain growth is governed by the drive energy and time, up to 155 μm. This length can be further increased by co-optimizing other drive parameters, such as wavelength, pulse width, repetition rate, etc. Furthermore, LDDG dramatically improves the processing efficiency of all-optical poling, which is one to two orders of magnitude faster than the laser scanning method for fabricating inverted domains in an $LiNbO_3$ crystal. 2D QPM of periodic structures fabricated using LDDG is presented. Our results open new avenues for optical poling with potential applications in nonlinear optics and domain wall motion.

Funding. National Natural Science Foundation of China (51727901); The Strategic Priority Research Program of the Chinese Academy of Sciences (XDA25040201).

Acknowledgments. We would like to acknowledge support from the Key Laboratory for Laser Plasmas (Ministry of Education).

Disclosures. The authors declare no conflicts of interest.

Data availability. Data underlying the results presented in this paper are not publicly available at this time but may be obtained from the authors upon reasonable request.

REFERENCES

1. X. Hong, B. Yang, C. Zhang, Y. Qin, and Y. Zhu, Phys. Rev. Lett. **113**, 163902 (2014).
2. K. Buse, A. Adibi, and D. Psaltis, Nature **393**, 665 (1998).
3. S. Y. Yang, J. Seidel, S. J. Byrnes, P. Shafer, C. H. Yang, M. D. Rossell, P. Yu, Y. H. Chu, J. F. Scott, J. W. Ager, L. W. Martin, and R. Ramesh, Nat. Nanotechnol. **5**, 143 (2010).
4. J. W. Lee, K. Eom, and T. R. Paudel, *et al.*, Nat. Commun. **12**, 8 (2021).
5. P. K. Chen, I. Briggs, S. Y. Hou, and L. R. Fan, Opt. Lett. **47**, 1506 (2022).
6. M. Höfling, X. D. Zhou, L. M. Riemer, E. Bruder, B. Z. Liu, L. Zhou, P. B. Groszewicz, F. P. Zhuo, B. X. Xu, K. Durst, X. L. Tan, D. Damjanovic, J. Koruza, and J. Rodel, Science **372**, 961 (2021).
7. L. E. Myers, R. C. Eckardt, M. M. Fejer, R. L. Byer, W. R. Bosenberg, and J. W. Pierce, J. Opt. Soc. Am. B **12**, 2102 (1995).
8. A. C. Muir, C. L. Sones, S. Mailis, R. W. Eason, T. Jungk, A. Hoffmann, and E. Soergel, Opt. Express **16**, 2336 (2008).
9. C. Y. J. Ying, A. C. Muir, C. E. Valdivia, H. Steigerwald, C. L. Sones, R. W. Eason, E. Soergel, and S. Mailis, Laser Photonics Rev. **6**, 526 (2012).
10. J. Guo, W. Chen, H. Chen, Y. Zhao, F. Dong, W. Liu, and Y. Zhang, Adv. Opt. Mater. **9**, 2002146 (2021).
11. A. Boes, H. Steigerwald, D. Yudistira, V. Sivan, S. Wade, S. Mailis, E. Soergel, and A. Mitchell, Appl. Phys. Lett. **105**, 092904 (2014).
12. H. Steigerwald, Y. J. Ying, R. W. Eason, K. Buse, S. Mailis, and E. Soergel, Appl. Phys. Lett. **98**, 062902 (2011).
13. B. Zhang, L. Wang, and F. Chen, Laser Photonics Rev. **14**, 1900407 (2020).
14. L. M. Mazur, S. Liu, X. Chen, W. Krolikowski, and Y. Sheng, Laser Photonics Rev. **15**, 2100088 (2021).
15. S. Liu, K. Switkowski, C. Xu, J. Tian, B. Wang, P. Lu, W. Krolikowski, and Y. Sheng, Nat. Commun. **10**, 3208 (2019).
16. T. Xu, K. Switkowski, X. Chen, S. Liu, K. Koynov, H. Yu, H. Zhang, J. Wang, Y. Sheng, and W. Krolikowski, Nat. Photonics **12**, 591 (2018).
17. X. Chen, D. W. Liu, S. Liu, L. M. Mazur, X. Liu, X. Y. Wei, Z. Xu, J. L. Wang, Y. Sheng, Z. Y. Wei, and W. Krolikowski, Adv. Opt. Mater. **10**, 2102115 (2022).
18. J. Imbrock, H. Hanafi, M. Ayoub, and C. Denz, Appl. Phys. Lett. **113**, 252901 (2018).
19. Y. Sheng, A. Best, H.-J. Butt, W. Krolikowski, A. Arie, and K. Koynov, Opt. Express **18**, 16539 (2010).
20. Y. Sheng, V. Roppo, K. Kalinowski, and W. Krolikowski, Opt. Lett. **37**, 3864 (2012).
21. R. Osellame, M. Lobino, N. Chiodo, M. Marangoni, G. Cerullo, R. Ramponi, H. T. Bookey, R. R. Thomson, N. D. Psaila, and A. K. Kar, Appl. Phys. Lett. **90**, 241107 (2007).
22. D. Wei, C. Wang, H. Wang, X. Hu, D. Wei, X. Fang, Y. Zhang, D. Wu, Y. Hue, J. Lie, S. Zhu, and M. Xiao, Nat. Photonics **12**, 596 (2018).
23. J. Thomas, V. Hilbert, R. Geiss, T. Pertsch, A. Tuennermann, and S. Nolte, Laser Photonics Rev. **7**, L17 (2013).
24. A. Agronin, M. Molotskii, Y. Rosenwaks, G. Rosenman, B. J. Rodriguez, A. I. Kingon, and A. Gruverman, J. Appl. Phys. **99**, 104102 (2006).
25. D. O. Alikin, A. V. Ievlev, A. P. Turygin, A. I. Lobov, S. V. Kalinin, and V. Y. Shur, Appl. Phys. Lett. **106**, 182902 (2015).
26. J. Park, Y. Ahn, J. A. Tilka, H. J. Lee, A. Pateras, M. H. Yusuf, M. Dawber, H. D. Wen, and P. G. Evans, Appl. Phys. Lett. **116**, 012901 (2020).
27. C. L. Sones, M. C. Wengler, C. E. Valdivia, S. Mailis, R. W. Eason, and K. Buse, Appl. Phys. Lett. **86**, 212901 (2005).
28. V. Y. Shur, D. K. Kuznetsov, E. A. Mingaliev, E. M. Yakunina, A. I. Lobov, and A. V. Ievlev, Appl. Phys. Lett. **99**, 082901 (2011).
29. M. Reich, F. Korte, C. Fallnich, H. Welling, and A. Tunnermann, Opt. Lett. **23**, 1817 (1998).
30. J. Imbrock, L. Wesemann, S. Kroesen, M. Ayoub, and C. Denz, Optica **7**, 28 (2020).
31. X. Chen, P. Karpinski, V. Shvedov, K. Koynov, B. Wang, J. Trull, C. Cojocaru, W. Krolikowski, and Y. Sheng, Appl. Phys. Lett. **107**, 141102 (2015).
32. X. Chen, P. Karpinski, V. Shvedov, A. Boes, A. Mitchell, W. Krolikowski, and Y. Sheng, Opt. Lett. **41**, 2410 (2016).